Materials Today Energy 33 (2023) 101270

Contents lists available at ScienceDirect

Materials Today Energy

journal homepage: www.journals.elsevier.com/materials-today-energy/

Effects of a high-performance, solution-cast composite electrolyte on the host electrospun polymer membrane for solid-state lithium metal batteries

Waqas Ul Arifeen [a,*], Zain Ul Abideen [b], Nunna Guru Parakash [a], Leng Xiaolong [a], Tae Jo Ko [a,**]

[a] School of Mechanical Engineering, Yeungnam University, Daehak-ro, Gyeongsan-si, Gyeongbuk-do, 38541, South Korea
[b] Research School of Chemistry, College of Science, Australian National University, Canberra, ACT, 2601, Australia

ARTICLE INFO

Article history:
Received 19 December 2022
Received in revised form
8 February 2023
Accepted 18 February 2023
Available online 24 February 2023

Keywords:
Solid-state electrolyte
Electrospun membrane
Solid-state batteries
Lithium batteries
Polymer electrolyte

ABSTRACT

Dispersed nano-silica fillers in poly (ethylene oxide) were solution cast on a host electrospun polyacrylonitrile membrane. The host electrospun polyacrylonitrile membrane enhanced the overall elasticity and ionic conductivity of the composite polymer electrolyte membrane for solid-state lithium metal batteries. Three different concentrations of silica fillers were added (1%, 3%, and 5%) called CSE 1, CSE 3, and CSE 5. The composite electrolyte membranes were compared with the 0% concentration of silica fillers and named SE. Among them, the CSE 3 membrane outperformed and delivered an ionic conductivity of 7.1×10^{-4} S cm^{-1}, lithium-ion transference number of 0.62, and the ultimate tensile strength of 27.3 MPa with 110.9% strain, revealing the elasticity of the CSE 3 membrane. The thermal stability of up to 354 °C and the wide range of electrochemical stabilities of up to 5.1 V were achieved. The symmetric cell Li|CSE 3|Li showed satisfactory long operation of lithium plating/stripping for 500 h without a significant voltage drop or short circuit. Furthermore, the electrode surface showed the homogeneous deposition of lithium on the plated electrode and a relatively smooth surface on the stripped electrode. The LCO|CSE 3|Li exhibits better rate capability and excellent cycling performance with 91.1% capacity retention and maintains 131.9 mAh g^{-1}at 0.5C after 200 cycles.

1. Introduction

Energy storage devices are the most significant components for practical applications, such as portable electronic devices and electric vehicles, which have increased the demand for high-energy-density storage systems [1–6]. Lithium-ion batteries are a promising candidate for advanced energy storage devices because of their low self-discharge behavior, long service life, large storage capacity, and high energy densities [7,8]. On the other hand, the energy density of commercial lithium-ion batteries with liquid electrolytes has reached 250 W h. kg^{-1}, which has limited some applications [9]. The conventional liquid electrolyte contains a combustible organic solvent, and the growth of lithium dendrites has safety issues during overcharging, such as thermal runaway, short circuits, and even fire risks. Therefore, the replacement of a liquid electrolyte with a solid-state electrolyte for lithium batteries is essential [10].

Solid-state electrolytes (SSEs) are the basic components of solid-state lithium metal batteries. Generally, SSEs can be categorized into solid polymer electrolytes (SPEs), solid composite electrolytes (SCEs), and inorganic ceramic electrolytes (ICEs). The SPEs contain the 3D polymer host matrices induced with the proportion of lithium salts and optimized with the introduction of plasticizers. The host polymer matrix provides robust mechanical strength, and dissolved lithium salt allows ion transportation. Consequently, the SPEs possess a wide window of electrochemical stability, and inferior thermal stability but present low ionic conductivity of less than 10^{-5} S cm^{-1}, and unsatisfactory action in suppressing dendritic growth [11–14]. A combination of inorganic fillers and SPEs fabricates the SCEs. Hence, they possess the combined efficiency, such as good flexibility, high ionic conductivity of greater than 10^{-5} S cm^{-1}, and provide greater contact with electrodes. On the

* Corresponding author.
** Corresponding author.
E-mail addresses: waqas@ynu.ac.kr (W.U. Arifeen), tjko@yu.ac.kr (T.J. Ko).

https://doi.org/10.1016/j.mtener.2023.101270
2468-6069/

other hand, ICEs exhibit a wider window of electrochemical stability, greater ionic conductivity of approximately 10^{-3} S cm^{-1}, and good mechanical strength [14]. SSEs are considered the best candidates for producing the next-generation lithium batteries because they reduce the drawbacks of liquid electrolytes, such as electrolyte leakage, toxicity, severe dendrite growth, and flammability. On the other hand, the ionic conduction between the anode and cathode is not as smooth as by liquid electrolyte because of the high interfacial resistance of the electrolyte/electrode due to the path of dry SSEs [12].

Polyethylene oxide (PEO), polyvinylidene fluoride (PVDF), polyacrylonitrile (PAN), and their subsequent derivatives have attracted enormous attention as SPEs owing to their good interfacial compatibility, high mechanical strength, potential high electrochemical stability, and excellent machinability [15,16]. PEO is one of the best candidates as the polymer host for SPEs because of its light weight, low cost, good miscibility with various lithium salts, low glass transition temperature, and high stability to lithium metal [17,18]. As the PEO structure is semi-crystalline, the PEO-based electrolyte shows poor conductivity of around 10^{-6}–10^{-8} S cm^{-1} at room temperature because of their inherently high degree of polymer crystallinity [19].

In this study, nano-silica fillers were dispersed in acetonitrile, followed by the dissolution of PEO containing a plasticizer EC and lithium salt $LiClO_4$. The resulting mixture was solution cast on a host electrospun PAN membrane. The host electrospun polyacrylonitrile membrane enhanced the overall elasticity and the ionic conductivity of the composite polymer electrolyte membrane for solid-state lithium metal batteries. Three different concentrations of silica fillers were added (0%, 1%, 3%, and 5%) and given the name SE, CSE 1, CSE 3, and CSE 5, respectively. The thermal stability, mechanical strength, ionic conductivity, and electrochemical stability of the prepared electrolyte membrane were studied. The lithium-ion transference number, lithium plating/stripping experiments, and cycling performance were investigated for the application of solid-state lithium metal batteries. Therefore, this type of PAN host polymer electrolyte membrane will be a developing direction of solid-state lithium metal batteries in the future.

2. Experimental section

2.1. Materials

PEO (M_W = 300,000), PAN (M_W = 150,000), N,N-dimethyl formamide (DMF), acetonitrile, ethylene carbonate (EC), lithium perchlorate ($LiClO_4$), and silicon dioxide 5–15 nm spherical particle size powder (SiO_2) were purchased from Sigma–Aldrich. Lithium cobalt dioxide ($LiCoO_2$) coated on aluminum foil called LCO, lithium metal chips (Li), stainless steel (SS) electrodes, and coin cell casings were purchased from MTI Korea. All the materials were used as received.

2.2. Synthesis of the electrolyte membrane

Firstly, 10 wt % of PAN was dissolved in DMF and stirred for six–eight hours to make it a homogeneous solution. The solution was loaded into a syringe fixed with an 18-gauge blunt end stainless steel (SS) needle. The syringe was mounted on a syringe pump placed 14 cm from the rotating drum. The PAN membrane was prepared by electrospinning. A high DC voltage of 20 kV was provided to the solution with a SS needle. The electrospun PAN membrane was attracted toward the electrically grounded rotating drum using an electrostatic force. The drum was rotated at a speed of 180 rpm. The electrospun membrane was collected on an aluminum foil wrapped on the rotating drum. The PAN membrane was placed in an oven overnight at 50 °C to ensure the PAN membrane was completely dry.

SiO_2 (SiO_2:PEO) at 1:10, 3:10, or 5:10 wt % was dispersed for 0.5 h in acetonitrile with sonication. $LiClO_4$ and EC at 15 wt % each were added to the solution and stirred for 2 h until a homogeneous solution. A 7:10 PEO (PEO:PAN) mixture was then added, and the resulting solution was stirred for five–six hours until a homogeneous solution formed. This solution was cast on the electrospun PAN membrane to obtain the composite electrolyte membrane embedded with the silica particles. The prepared electrolyte membrane was then placed overnight in an oven at 50 °C to ensure the removal of the residual solvent. The prepared electrolyte membrane was peeled off from the aluminum foil for further examination. Fig. 1 presents the overall schematic diagram of the prepared electrolyte membrane. The membranes with 0%, 1%, 3%, and 5% SiO_2 nanoparticles were named SE, CSE 1, CSE 3, and CSE 5, respectively.

2.3. Physico-chemical characterization of the electrolyte membrane

The morphology of the SE and CSE membranes was examined by field emission scanning electron microscopy (FE SEM S-4800, Hitachi Ltd.). Image J software was used to calculate the diameter of the SE and CSE membranes. X-ray diffraction (XRD, DIATOME) was carried out to analyze the crystallinity of the electrolyte

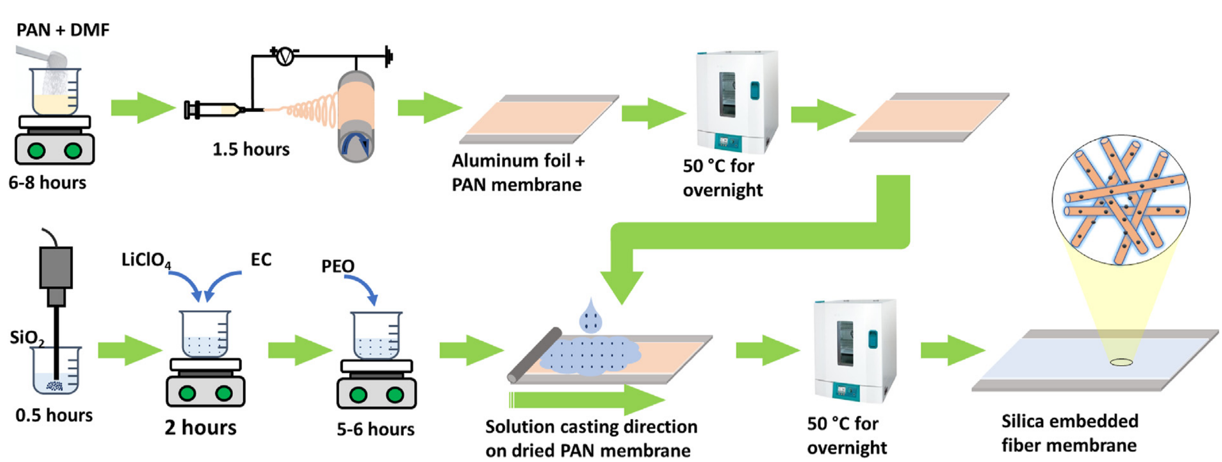

Fig. 1. Schematic illustration for the preparation of electrolyte membranes.

membranes using Cu Kα radiation (λ = 1.54 Å) between 10° and 80° 2θ. The chemical bonding structure was examined by Fourier transform infrared (FTIR) spectroscopy. The thermal stability test was analyzed by thermogravimetric analysis (TGA, SDT-Q600, TA Instruments, USA) under the temperature range of 25–700 °C with a heat flow rate of 10 °C.min^{-1}. The mechanical strength of the electrolyte membranes was analyzed using a universal testing system (UTS) machine (Instron 3365).

2.4. Electrochemical characterization of the electrolyte membrane

The electrolyte membranes were sandwiched between SS electrodes in a symmetric cell to examine the ionic conductivity of the electrolyte membranes. The bulk resistance (R) of the electrolyte membrane was evaluated from Nyquist plots from alternating current (AC) impedance analysis with AC amplitude of 3 mV and frequency range of 100 kHz and 1 Hz using an electrochemical workstation (SP-200 potentiostat, Biologic). The ionic conductivity (σ) was calculated using equation (1)

$$\sigma = \frac{t}{RA} \quad (1)$$

where t is the thickness, and A is the electrolyte membrane area. The electrochemical stability of the electrolyte membranes was evaluated by linear sweep voltammetry (LSV) from the voltage window of 2.0–6.5 V with a scan rate of 1.0 mVs^{-1}. The electrolyte membranes were assembled between SS and Li for LSV. The reversibility and cut-off voltage for the electrolyte membranes

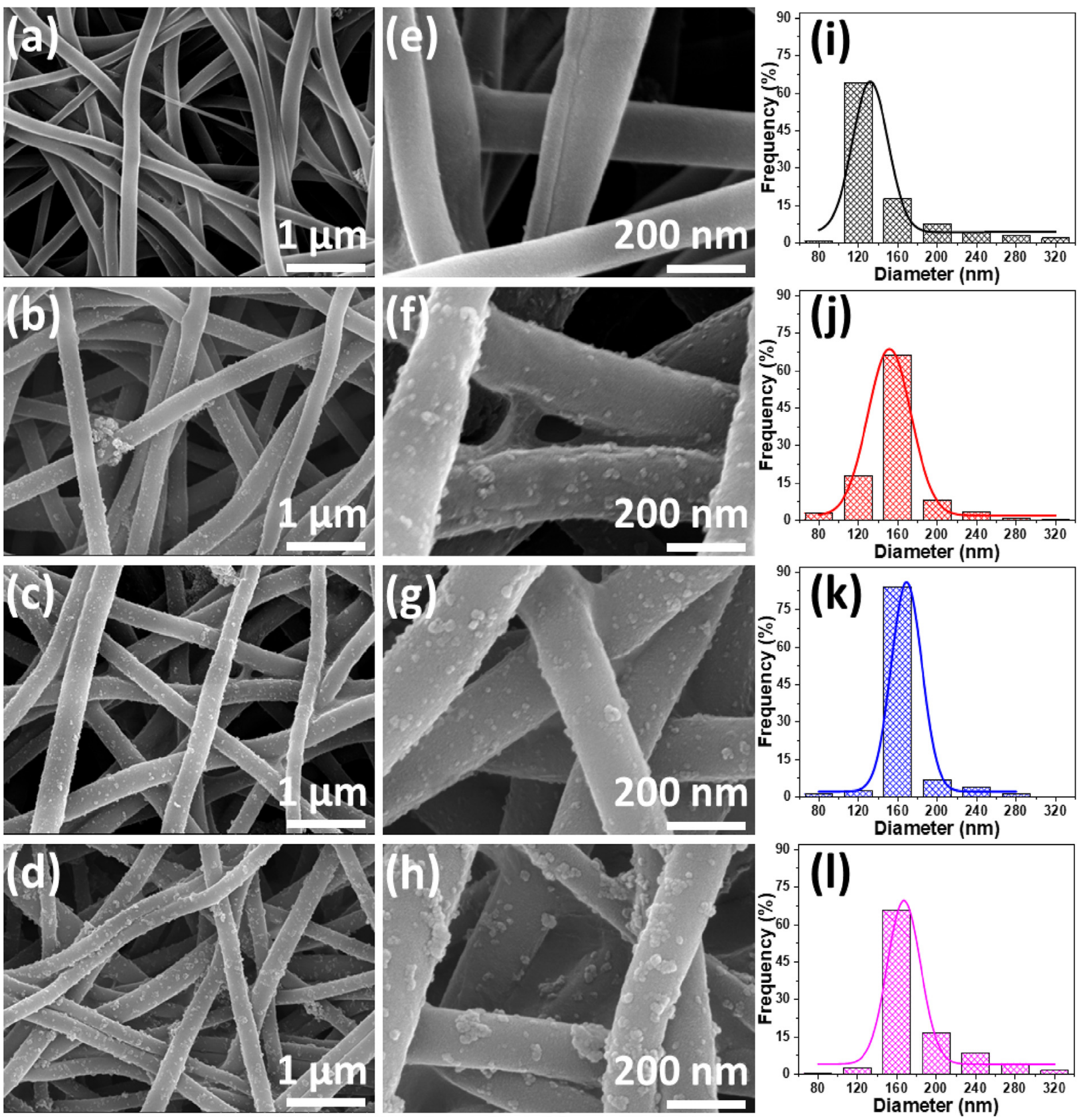

Fig. 2. (a), (b), (c), and (d) are the SEM images on lower magnification representing the continuity and uniformity of the electrolyte membrane, (e), (f), (g), and (h) are the SEM images on higher magnification represents the addition of PEO and silica particles with the solution casting method, (i), (j), (k) and (l) represents the distribution frequency of the diameter for SE, CSE 1, CSE 3, and CSE 5, respectively.

were studied by cyclic voltammetry (CV) curves with a voltage window of 2.0–4.3 V with a scan rate of 1.0 mVs^{-1}. The electrolyte membrane was assembled between LCO and Li for CV. The lithium-ion transfer number (t_{Li^+}) was investigated by the AC impedance spectrum and the chronoamperometry test and calculated according to the Bruce–Vincent equation (2)

$$t_{Li^+} = \frac{I_S(\Delta V - I_0 R_0)}{I_0(\Delta V - I_S R_S)} \tag{2}$$

where ΔV is the DC voltage, R_0 and R_S are the interfacial resistances before and after the chronoamperometry test, respectively, and I_0 and I_S are the current in the initial and steady states, respectively. The electrolyte membrane was assembled between a Li symmetric cell for chronoamperometry.

The electrochemical compatibility of the electrolyte membrane with Li plating/stripping metal was investigated from the galvanostatic charge/discharge voltage profiles with a current density of 0.1 mA cm^{-2} for 500 h. The electrolyte membrane was assembled between Li symmetric cells for the Li plating/stripping test. For further battery test evaluations of the electrolyte membrane, the charge/discharge cycles were performed with different current rates of 0.1C–5C. The discharge capacity for 200 cycles was investigated with a current rate of 0.5C. The electrolyte membrane was assembled between LCO and Li for the battery tests. The cells for electrochemical characterization of the electrolyte membranes were prepared in an argon-filled glove box.

3. Results and discussion

Fig. 2 presents the detailed morphology of the electrolyte membranes. Fig. 2 (a) and (e) represent an SEM image of the SE, where a PEO solution containing EC and $LiClO_4$ was cast on the host PAN membrane. The image shows no silica content on the SE fibers. The overall fiber diameter distribution is uniform, and more than 60% of the fiber diameter was ~ 120 nm, as shown in Fig. 2 (i). Fig. 2 (b) and (f) show SEM images of CSE 1; (c) and (g) present the SEM images of CSE 3; (d) and (h) show SEM images of CSE 5. The layer-by-layer randomly overlaid electrospun host PAN membranes showed a uniform distribution of fibers, which is vital for the mechanical strength and ionic conductivity of the electrolyte membranes. On the other hand, a small portion of agglomerated unwanted SiO_2 particles may cause resistance in the flow of ions between the electrodes during the charging and discharging processes. The proper dispersion of silica can avoid this. In this study, the optimized concentration of silica was in the range of 1–5%. Fig. 2 (f), (g), and (h) present solution-cast PEO with various silica concentrations. Adding silica to PEO improved the mechanical strength, thermal stability, and ionic conductivity. Fig. 2 (j), (k), and (l) show the fiber diameter of CSE1, CSE 2, and CSE 3, respectively. The overall fiber distribution was ~160 nm which was calculated using Image J software from SEM. In the case of CSE 1, more than 60% of the fibers were approximately 160 nm in diameter, and 15% of the fibers were 120 nm. In the case of CSE 5, 15% of the fibers were approximately 200 nm in diameter, and approximately 60% of the fibers were 160 nm in diameter. More than 80% of the fibers were ~160 nm in the case of CSE 3, which shows a more uniform diameter distribution of fibers.

Fig. 3 (a) presents the XRD patterns of the electrolyte membranes with different silica compositions to show the crystallinity of the prepared electrolyte membranes. The peak at 17° is attributed to the crystalline part whereas the broad peak at 26° is attributed to the enhanced amorphous region of the pure electrospun PAN membrane as shown in Fig. 3 (a) (dotted line) [20]. The strong characteristic peaks at 19° and 23° is attributed to the high crystalline region of PEO as shown in Fig. 3 (a) (dashed line). The high crystalline tendency of the pure PEO decreased considerably with the addition of $LiClO_4$ and the host electrospun PAN in the SE curve. The PEO crystalline peak intensity was further decreased with the addition of silica [16], as shown in the CSE 1, CSE 3, and CSE 5 curves in Fig. 3 (a); however, the silica concentration did not affect the crystallinity of the membranes, which were semi-crystalline or a co-existence of crystalline and amorphous regions. The XRD patterns show that the polymer electrolyte membranes were amorphous, which allows more ion transportation through the membranes.

Fig. 3 (b) presents the FTIR spectrum of the electrolyte membranes. The FTIR spectrum of the SE membrane represents the characteristic bands of PAN at 2890 cm^{-1} and 1466 cm^{-1} observed from the asymmetric bending and stretching of the CH_2 and 1340 cm^{-1} from CH bending [6]. The peaks at 840 cm^{-1} and 960 cm^{-1} were assigned to the C–H bond of the C=CH_2 group. The absorbance at 1280 cm^{-1} was attributed to the C=O due to ester formation in PEO. These peaks are also visible in the CSE membranes. On the other hand, the characteristic peaks near 620 cm^{-1} and 1080 cm^{-1} are an indication of Si–O–Si skeleton formation, and the broader peak near 3500 cm^{-1} is assigned to silanol or free hydroxyl group (O–H) in the SiO_2 [21]. The new formation of double peaks at 1790 cm^{-1} represents the existence of both nitrile group (–C≡N) due to PAN and carbonyl group (–C=O) due to polymerization of PEO in the composite membranes [22].

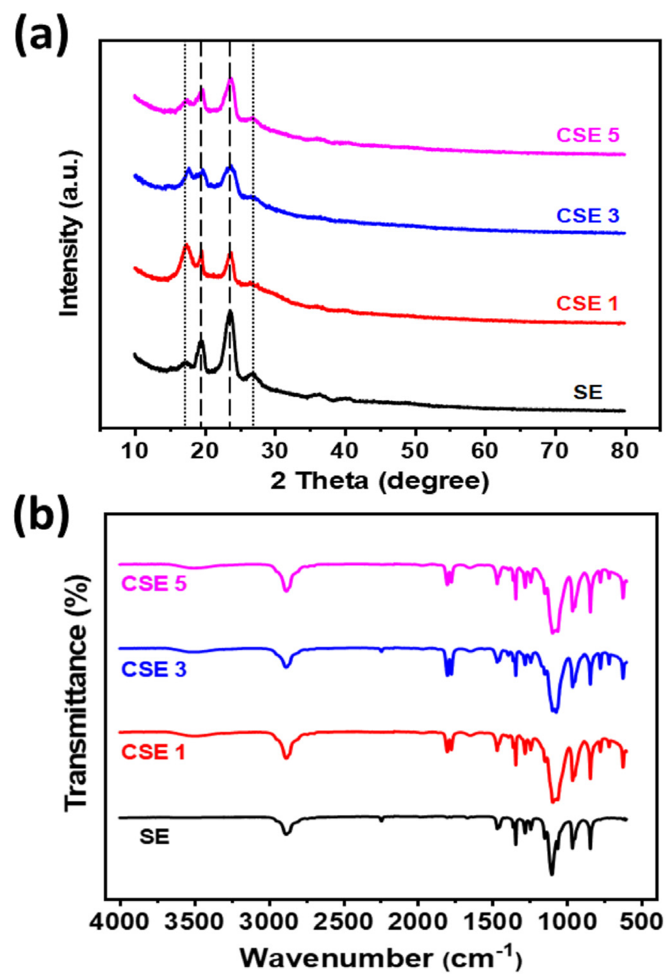

Fig. 3. (a) XRD curves and (b) FTIR spectrum of the electrolyte membranes.

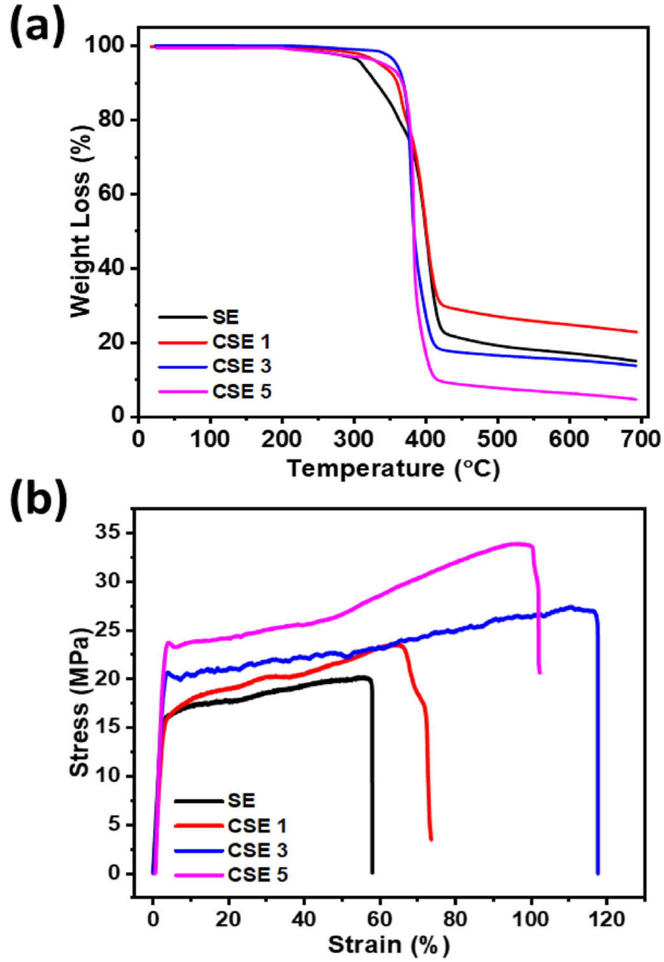

Fig. 4. (a) TGA curves and (b) Mechanical strength analysis of the electrolyte membranes.

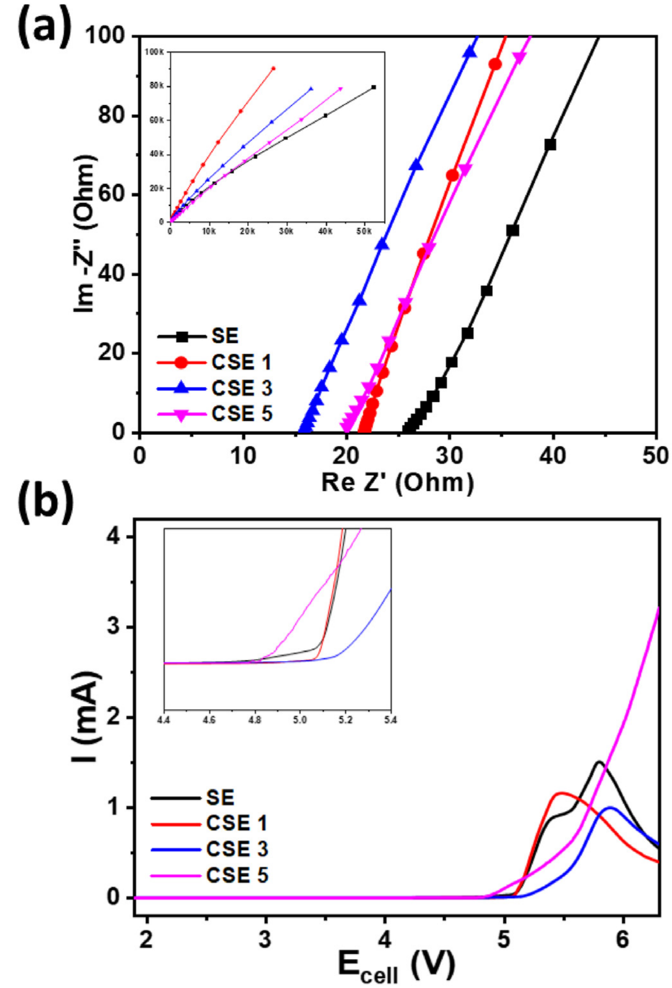

Fig. 5. (a) The Nyquist plots and (b) LSV curves of the various electrolyte membranes.

Fig. 4 (a) represents the TGA results of the electrolyte membranes in the temperature range of up to 700 °C. The temperature was increased from room temperature to 700 °C at 10 °C/min in a nitrogen atmosphere. The SE membrane started decomposition from 97 wt % at 301 °C, which is the melting temperature of PAN, to 23 wt % at 422 °C. On the other hand, CSE 1, CSE 3, and CSE 5 started decomposition from 97 wt % at 354 °C, which was higher than the melting temperature of the host electrospun PAN membrane. This improvement in temperature stability was attributed to the addition of silica particles, and the whole membrane samples decomposed at 412 °C. The weight remaining the 700 °C was traces of carbon and silica particles, which comprised 10–20 wt % of the original samples [23]. Fig. 4 (b) reveals the stress–strain curves of the electrolyte membranes. The SE and CSE 1 membranes showed a yield strength of 16.3 MPa, while CSE 3 and CSE 5 had yield strengths of 20.5 and 23.6 MPa, respectively. Adding the solution-cast PEO containing silica to the host electrospun PAN membrane enhanced the yield strength of the electrolyte membranes. The ultimate tensile strength of CSE 3 is 27.3 MPa with a strain of 110.9%. The stress–strain curves also revealed the elastic nature of the electrolyte membranes. All the composite membranes showed a higher ultimate strength than the yield strength with more than 70% of the strain, i.e., all the electrolyte membranes are elastic. One of the reasons for the elasticity is that the host polymer membrane is electrospun PAN, which provides strength and strain simultaneously to the overall electrolyte membrane.

The ionic conductivities (σ) of the electrolyte membranes were 3.6×10^{-4} S cm^{-1} for SE and 4.3×10^{-4} S cm^{-1}, 7.1×10^{-4} S cm^{-1}, and 4.0×10^{-4} S cm^{-1} for CSE 1, CSE 3, and CSE 5 assembled coin cell membranes, respectively. Fig. 5 (a) presents Nyquist plots of the bulk resistances and the corresponding ionic conductivities calculated using Eq. (1). One of the strategies to obtain high ionic conductivity was to prepare porous electrospun PAN membranes. Therefore, the high ionic conductivities in the composite electrolyte membranes can explain the host electrospun PAN membrane, which is amorphous as confirmed by XRD, and the elastic nature confirmed from the stress–strain curves. Fig. 5 (b) shows the electrochemical stability of the electrolyte membranes. The excess silica concentration causes an early oxidation current at 4.8 V for the CSE 5 membrane (Fig. 5 (b) inset). On the other hand, the electrochemical window is still wide and stable enough compared to the commercial liquid electrolyte LIBs, which have a working voltage range of approximately 4.2–4.3 V [24]. The wide range of electrochemical voltage window for CSE 1 and CSE 3 electrolyte membranes of up to 5.0 and 5.1 V, respectively, indicates that the slight concentration of silica helped stabilize the breakdown

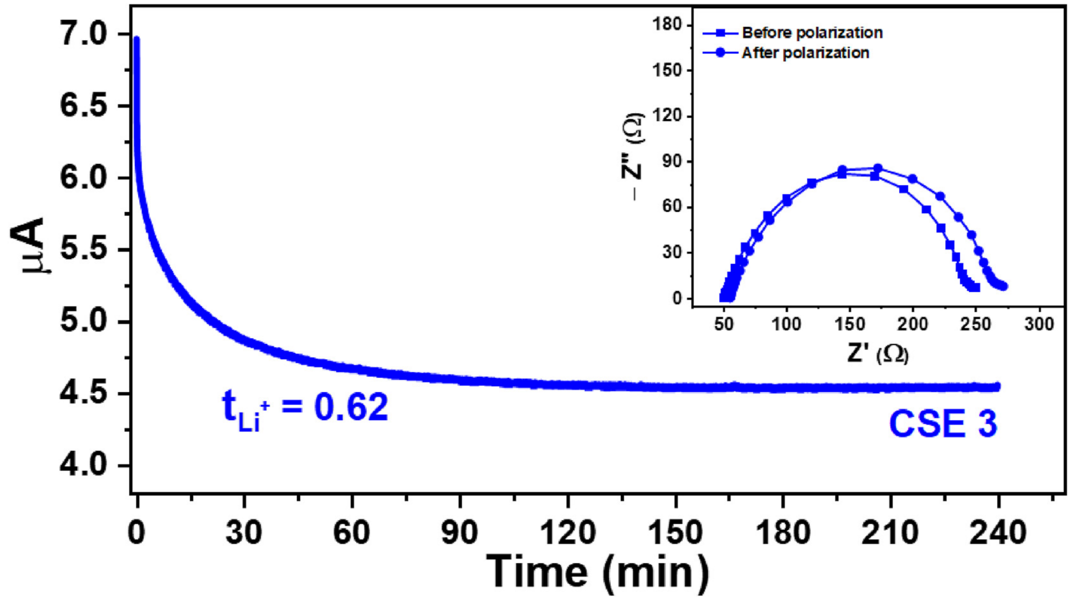

Fig. 6. DC polarization of Li|CSE 3|Li coin cell and (inset) the AC impedance curve before and after polarization.

voltage at a higher range, which means the membranes can meet the requirements of most high voltage cathode materials, such as LCO. The CV curves are represented in Figure S1 (supplementary information). There was a continuous increasing current flowing in the case of the SE, CSE 1, and CSE 5 electrolyte membranes, indicating the continuous oxidation process occurring in the 10 consecutive cycles of CV. The oxidation and reduction peaks were observed at 4.1 V and 3.6 V, respectively, in the case of CSE 3

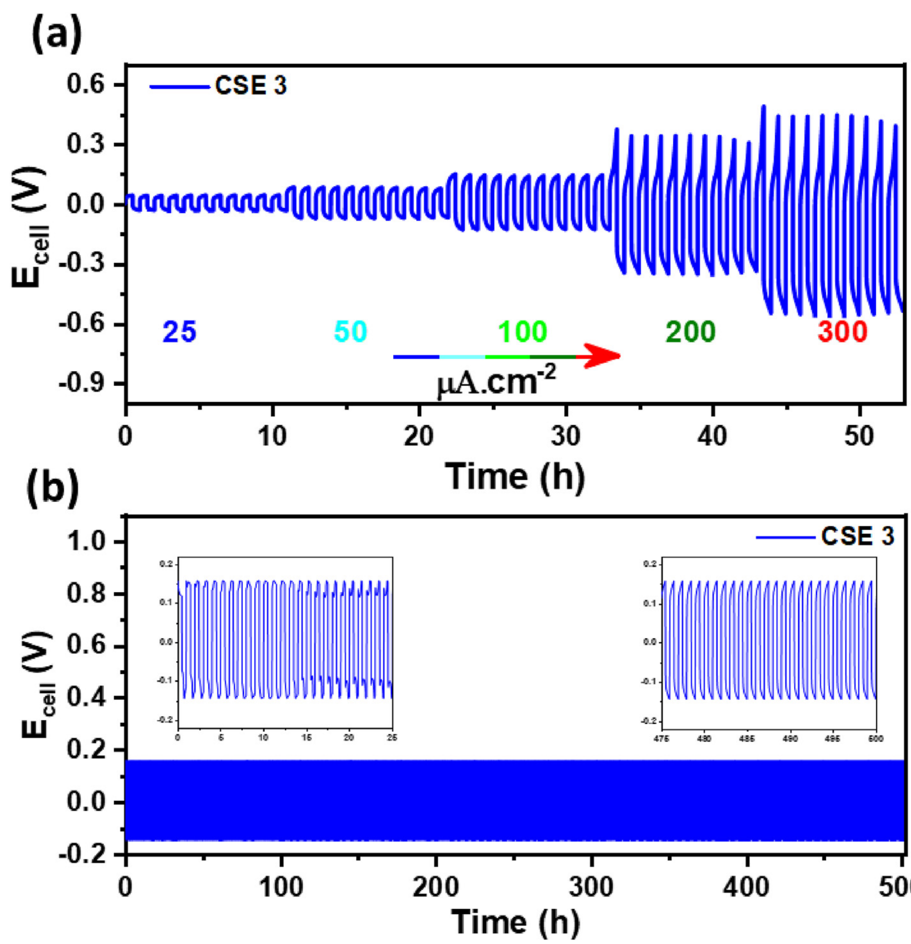

Fig. 7. Lithium plating-stripping experiment of CSE 3 assembled in symmetric lithium electrodes (a) various C rates ranging from 25 to 300 μA cm^{-2} (b) 500 cycles with 100 μA cm^{-2} with voltage profiles from 0 to 25 and 475–500 cycles in the inset.

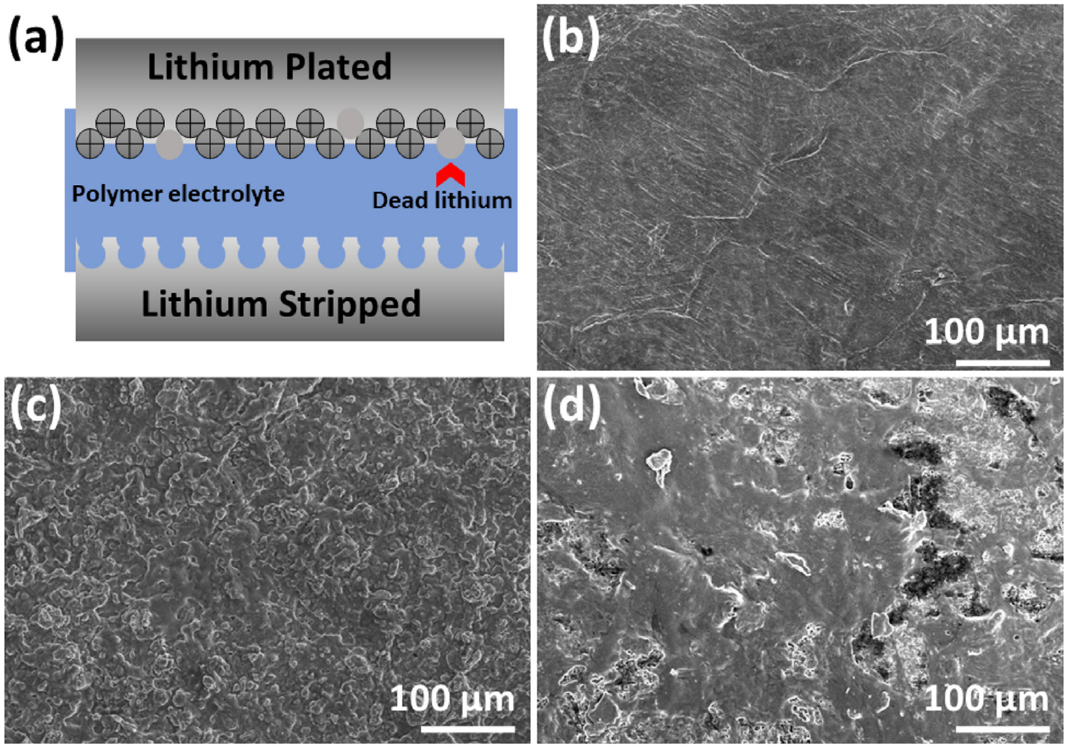

Fig. 8. (a) Schematic lithium plated-stripped electrodes (b) Unused lithium electrode surface (c) plated and (d) stripped electrode analysis after 500 lithium plating-stripping cycles assembled with CSE 3 by SEM image.

throughout 10 cycles. No impurity peaks were observed in the batteries, indicating no side reactions and uniform reversibility of the electrodes in the presence of prepared electrolyte membranes.

The t_{Li^+} is a vital factor of SPEs. Equation (2) was used to calculate t_{Li^+}. Table S2 lists the current-time curves of the DC polarization (initial and steady-state current) and the interfacial resistances of the AC impedance spectrum before and after DC polarization. t_{Li^+} of the prepared electrolyte membrane were calculated to be 0.31, 0.43, 0.62, and 0.38 for SE, CSE 1, CSE 3, and CSE 5, respectively. Fig. 6 presents the DC polarization of CSE 3 and the AC impedance before and after DC polarization. The t_{Li^+} of CSE 3 was 0.62, which is much higher than those of the SE, CSE 1, and CSE 5, indicating that the slight addition of PEO-SiO_2 on the host electrospun PAN membrane makes the semi-crystalline structure and allows easy Li^+ transportation due to the co-existence of crystalline and amorphous regions. On the other hand, the increase in SiO_2 concentration causes agglomeration in the path of Li^+ diffusion that blocks the transport of Li^+ ions, which concurs with the XRD and Nyquist plots.

The rate performance of the Li plating/stripping was examined by the galvanostatic cycling tests with a successive increase in current density of 25, 50, 100, 200, and 300 μA cm^{-2} (10 cycles each) followed by 500 cycles with a constant current density of 100 μA cm^{-2} to assess the feasibility of CSE 3 in a solid-state lithium battery. The best performance was achieved using the CSE 3 (3% silica content) membrane because of the absence of dendrite formation and reflecting the good conductive properties. Fig. 7 (a) shows the voltage profile of the Li plating/stripping test of CSE 3 with various current densities from 25 to 300 μA cm^{-2}. The CSE 3 membrane cell can maintain the increasing voltage polarization of 45, 85, 140, 330, and 550 mV at 25, 50, 100, 200, and 300 μA cm^{-2} with the relevant stability of the Li/electrolyte interphase, which may promote the safety of the CSE 3 membrane, even at higher current densities. The cell comprised of the CSE 3 membrane was sustained during the long cycles of 500 h at 100 μA cm^{-2}, as shown in Fig. 7 (b), and a negligible voltage drop was observed. The voltage profiles of the CSE 3 membrane showed similar behavior to that at the beginning of the test, as shown in the inset of Fig. 7 (b). The low crystallinity and good dispersion of silica particles in the host electrospun PAN membrane led to the uniform transportation of Li^+ during long-term cycling, suggesting the stable and good compatibility of the CSE 3 membrane with the electrodes. The cell comprised of the SE membrane showed a short-circuit at 300 cycles, as shown in Fig. S3, the voltage drop of 0.04 mV was observed in the case of the CSE 1 membrane cell, as shown in Fig. S4, and the cell comprised of the CSE 5 membrane showed missing cycles at 250 cycles, as shown in Fig. S5 (inset), which confirms the agglomeration of silica particles resulting in the blockage of Li^+ migration. Fig. 8 (a), (b), (c), and (d) presents a schematic diagram of plated and stripped lithium electrodes, unused lithium electrode, and the surface morphology of the corresponding lithium electrodes used in a coin cell of the CSE 3 membrane, respectively. The addition of 3% silica particles helped enhance the ionic conductivity and lithium-ion transference number, which resulted in uniform deposition on the plated-stripped electrode surface with no dendrite growth on either surface of the electrode despite the total of 500 cycles (Fig. 8 (c), (d)). In contrast, the lithium electrodes cycled with the SE, CSE 1, and CSE 5 electrolyte membranes showed rough, uneven, and dead lithium particles with cracks on the plated surface of the

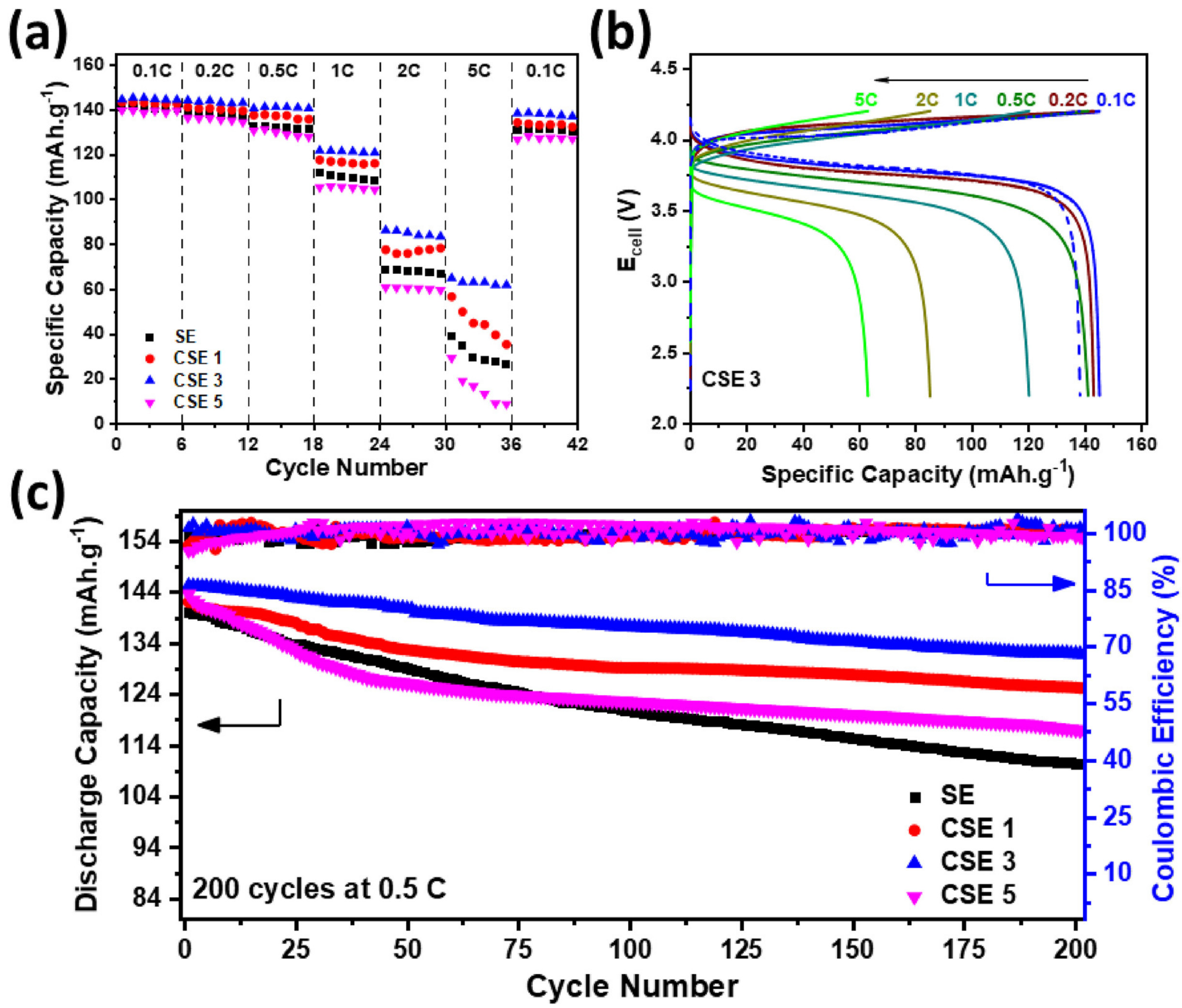

Fig. 9. (a) Specific capacity with various current rates from 0.1C to 5C and then back to 0.1C, (b) voltage plateau vs specific capacity of the CSE 3 membrane with various current rates and (c) the discharge capacity and coulombic efficiency of the coin cell assembled with SE, CSE 1, CSE 3 and CSE 5.

electrodes, while uneven grids, inhomogeneous lithium metal extraction was observed on the surface of the stripped electrodes (Fig. S6).

The prepared SE, CSE 1, CSE 3, and CSE 5 electrolyte membranes were assembled in LCO//Li electrodes for further investigation of battery tests. Fig. 9 (a) presents the rate capability of all the prepared electrolyte membranes assembled in a full cell when cycling with various current rates of 0.1, 0.2, 0.5, 1, 2, 5, and 0.1 C, respectively. The LCO/CSE 3/Li cell delivered a discharge capacity of 144.9, 142.8, 140.5, 121, 84.9, and 61.8 mAh g^{-1} at 0.1, 0.2, 0.5, 1, 2, and 5C, respectively, and returned to high discharge capacity of 137.1 mAh g^{-1} at 0.1C showing a better rate capability because of high ionic conductivity and better Li^+ transference number. On the other hand, the rate capability from 141.3 to 130.4 mAh g^{-1}, 142.9 to 132 mAh g^{-1}, and 139.3 to 126.6 mAh g^{-1} was delivered by LCO/SE/Li, LCO/CSE 1/Li, and LCO/CSE 5/Li cell, respectively. The cell assembled with the CSE 5 membrane delivered a very low discharge capacity of 139.3 mAh g^{-1} at 0.1C, 8 mAh g^{-1} at 5C, and a rate capability of 126.6 mAh g^{-1} at 0.1C (Fig. 9 (a)) because of the high concentration of silica, which caused agglomeration and blockage of Li^+. Fig. 9 (b) presents the corresponding selective voltage profiles of the CSE 3 membrane at various charge/discharge current rates of the rate capability. Although the discharge capacity of the recovered rate capability was less than that of 0.5C, the voltage profile decreased continuously from 0.1C to 5C. On the other hand, the voltage profile was recovered in the later 0.1C discharge profile, which is represented as the dashed line shown in Fig. 9 (b). The voltage profile also validated the results of lithium plating-stripping experiments, where a negligible voltage drop was observed in the long cycling of 500 cycles, as shown in Fig. 7 (b). In addition, the self-healing behavior of the silica concentration was observed in the galvanostatic cycling and charge/discharge cycles at various current rates, as reported elsewhere [9]. In contrast, the voltage profile could not maintain its original pattern at a high current rate of 2C and 5C in the case of the SE, CSE 1, and CSE 5 membranes, as shown in Fig. S7.

The cycling performance of the prepared electrolyte membrane assembled in LCO//Li was investigated at a 0.5C rate for 200 cycles, as shown in Fig. 9 (c). The cells assembled with SE, CSE 1, and CSE 5 membranes delivered the discharge capacity of 110.5, 125.2, and 117 mAh g^{-1} at the end of 200 cycles, corresponding to a 78.9%, 88.1%, and 81.8% of capacity retention, respectively. On the other hand, the cells delivered 100% coulombic efficiency despite the decreasing trend of their discharge capacity. In comparison, the cell assembled with the CSE 3 membrane maintained the discharge capacity of 131.9 mAh g^{-1} at the end of 200 cycles, retaining 91.1%

of its initial discharge capacity and representing 100% coulombic efficiency. A sudden drop of discharge capacity was noted in the first 70 cycles of all cells except for the CSE 1 and CSE 3 cells, confirming the good interfacial stability of electrolyte/electrodes, as shown in Fig. S6 (c, d) and Fig. 8 (c, d) respectively. The CSE 1 and CSE 3 membrane cells delivered better capacity retention because of their better interfacial stability. Nevertheless, the SE and CSE 5 membranes showed a considerable decrease in discharge capacity in the first 70 cycles and maintained a low-capacity retention of 78.9% and 81.8%, respectively.

4. Conclusion

PEO containing dispersed silica fillers was solution cast on a host electrospun membrane, to prepare a novel composite solid electrolyte for solid-state lithium metal batteries. The semi-crystalline composite electrolyte membrane showed remarkable improvements in the thermal stability of up to 354 °C, a mechanical strength of up to 20.5 MPa, ionic conductivity of 7.1×10^{-4} S cm^{-1}, . and a wide electrochemical window of 5.1 V with a high lithium transference number of 0.62. The symmetric Li|CSE 3|Li delivered the 500 cycles of galvanostatic cycling with a negligible voltage drop, representing the good interfacial stability of the electrode/electrolyte and the dendrite-free electrode surface. In addition, the LCO|CSE 3|Li exhibited excellent reversibility of 10 CV cycles, outstanding rate capability of 137.1 mAh g^{-1}, and superior capacity retention of 91.1% after 200 cycles at 0.5C with a remaining discharge capacity of 131.9 mAh g^{-1}. Therefore, this work provides great potential for composite polymer electrolytes for all solid-state lithium metal batteries at room temperature.

Credit author statement

Waqas Ul Arifeen: Conceptualization, Methodology, Validation, Formal analysis, Investigation, Data curation, Writing – Original Draft, Writing – Review & Editing, Visualization.
Zain Ul Abideen: Writing – Review & Editing, Visualization.
Nunna Guru Parakash: Investigation.
Xiaolong Leng: Software.
Tae Jo Ko: Validation, Resources, Writing – Review & Editing, Supervision, Project administration, Funding acquisition.

Declaration of competing interest

The authors declare that they have no known competing financial interests or personal relationships that could have appeared to influence the work reported in this paper.

Data availability

Data will be made available on request.

Acknowledgment

This study was supported by the Basic Science Program through the National Research Foundation of Korea (NRF) and funded by the Ministry of Education (NRF-2020R1A4A1019227).

Appendix A. Supplementary data

Supplementary data to this article can be found online at https://doi.org/10.1016/j.mtener.2023.101270.

References

[1] W.U. Arifeen, M. Kim, J. Choi, K. Yoo, R. Kurniawan, T.J. Ko, Optimization of porosity and tensile strength of electrospun polyacrylonitrile nanofibrous membranes, Mater. Chem. Phys. 229 (2019), https://doi.org/10.1016/j.matchemphys.2019.03.020.
[2] W.U. Arifeen, M. Kim, D. Ting, R. Kurniawan, J. Choi, K. Yoo, T.J. Ko, Hybrid thermal resistant electrospun polymer membrane as the separator of lithium ion batteries, Mater. Chem. Phys. 245 (2020), https://doi.org/10.1016/j.matchemphys.2020.122780.
[3] T. Dong, W.U. Arifeen, M. Kim, J. Choi, K. Yoo, T.J. Ko, Membranes made from electrospun polyacrylonitrile nonwoven fibers with uniform diameter for lithium-ion battery separators, Fibers Polym. 21 (2020), https://doi.org/10.1007/s12221-020-1243-4.
[4] T. Dong, W.U. Arifeen, J. Choi, K. Yoo, T. Ko, Surface-modified electrospun polyacrylonitrile nano-membrane for a lithium-ion battery separator based on phase separation mechanism, Chem. Eng. J. 398 (2020), https://doi.org/10.1016/j.cej.2020.125646.
[5] X. Leng, M. Yang, C. Li, W.U. Arifeen, T.J. Ko, High-performance separator for lithium-ion battery based on dual-hybridizing of materials and processes, Chem. Eng. J. (2021), https://doi.org/10.1016/j.cej.2021.133773.
[6] W.U. Arifeen, J. Choi, K. Yoo, J. Shim, T.J. Ko, A nano-silica/polyacrylonitrile/polyimide composite separator for advanced fast charging lithium-ion batteries, Chem. Eng. J. 417 (2021), https://doi.org/10.1016/j.cej.2020.128075.
[7] L. Zhu, J. Li, Y. Jia, P. Zhu, M. Jing, S. Yao, X. Shen, S. Li, F. Tu, Toward high performance solid-state lithium-ion battery with a promising PEO/PPC blend solid polymer electrolyte, Int. J. Energy Res. 44 (2020) 10168–10178, https://doi.org/10.1002/er.5632.
[8] Q. Liu, Y. Liu, X. Jiao, Z. Song, M. Sadd, X. Xu, A. Matic, S. Xiong, J. Song, Enhanced ionic conductivity and interface stability of hybrid solid-state polymer electrolyte for rechargeable lithium metal batteries, Energy Storage Mater. 23 (2019) 105–111, https://doi.org/10.1016/j.ensm.2019.05.023.
[9] L. Mezzomo, S. Bonato, S. Mostoni, B. Di Credico, R. Scotti, M. D'Arienzo, P. Mustarelli, R. Ruffo, Composite solid-state electrolyte based on hybrid poly(ethylene glycol)-silica fillers enabling long-life lithium metal batteries, Electrochim. Acta 411 (2022), https://doi.org/10.1016/j.electacta.2022.140060.
[10] B. Yuan, B. Zhao, Q. Wang, Y. Bai, Z. Cheng, Z. Cong, Y. Lu, F. Ji, F. Shen, P.F. Wang, X. Han, A thin composite polymer electrolyte with high room-temperature conductivity enables mass production for solid-state lithium-metal batteries, Energy Storage Mater. 47 (2022) 288–296, https://doi.org/10.1016/j.ensm.2022.01.052.
[11] V. Marangon, Y. Tominaga, J. Hassoun, An alternative composite polymer electrolyte for high performances lithium battery, J. Power Sources 449 (2020), https://doi.org/10.1016/j.jpowsour.2019.227508.
[12] J. Wang, S. Li, Q. Zhao, C. Song, Z. Xue, Structure code for advanced polymer electrolyte in lithium-ion batteries, Adv. Funct. Mater. 31 (2021), https://doi.org/10.1002/adfm.202008208.
[13] H. Liang, M. Zarrabeitia, Z. Chen, S. Jovanovic, S. Merz, J. Granwehr, S. Passerini, D. Bresser, Polysiloxane-based single-ion conducting polymer blend electrolyte comprising small-molecule organic carbonates for high-energy and high-power lithium-metal batteries, Adv. Energy Mater. (2022), 2200013, https://doi.org/10.1002/aenm.202200013.
[14] S. Li, S.Q. Zhang, L. Shen, Q. Liu, J. Bin Ma, W. Lv, Y.B. He, Q.H. Yang, Progress and perspective of ceramic/polymer composite solid electrolytes for lithium batteries, Adv. Sci. 7 (2020), https://doi.org/10.1002/advs.201903088.
[15] W. Bao, Z. Hu, Y. Wang, J. Jiang, S. Huo, W. Fan, W. Chen, X. Jing, X. Long, Y. Zhang, Poly(ionic liquid)-functionalized graphene oxide towards ambient temperature operation of all-solid-state PEO-based polymer electrolyte lithium metal batteries, Chem. Eng. J. 437 (2022), 135420, https://doi.org/10.1016/j.cej.2022.135420.
[16] D. Lin, W. Liu, Y. Liu, H.R. Lee, P.C. Hsu, K. Liu, Y. Cui, High ionic conductivity of composite solid polymer electrolyte via in situ synthesis of monodispersed SiO2 nanospheres in poly(ethylene oxide), Nano Lett. 16 (2016) 459–465, https://doi.org/10.1021/acs.nanolett.5b04117.
[17] Y. Li, L. Zhang, Z. Sun, G. Gao, S. Lu, M. Zhu, Y. Zhang, Z. Jia, C. Xiao, H. Bu, K. Xi, S. Ding, Hexagonal boron nitride induces anion trapping in a polyethylene oxide based solid polymer electrolyte for lithium dendrite inhibition, J. Mater. Chem. A. 8 (2020) 9579–9589, https://doi.org/10.1039/d0ta03677c.
[18] W.Q. Ding, F. Lv, N. Xu, M.T. Wu, J. Liu, X.P. Gao, Polyethylene oxide-based solid-state composite polymer electrolytes for rechargeable lithium batteries, ACS Appl. Energy Mater. 4 (2021) 4581–4601, https://doi.org/10.1021/acsaem.1c00216.
[19] Y. Li, Z. Sun, D. Liu, Y. Gao, Y. Wang, H. Bu, M. Li, Y. Zhang, G. Gao, S. Ding, A composite solid polymer electrolyte incorporating MnO2 nanosheets with reinforced mechanical properties and electrochemical stability for lithium metal batteries, J. Mater. Chem. A. 8 (2020) 2021–2032, https://doi.org/10.1039/c9ta11542k.
[20] M. Yanilmaz, Y. Lu, J. Zhu, X. Zhang, Silica/polyacrylonitrile hybrid nanofiber membrane separators via sol-gel and electrospinning techniques for lithium-ion batteries, J. Power Sources 313 (2016) 205–212, https://doi.org/10.1016/J.JPOWSOUR.2016.02.089.
[21] M. Yanilmaz, Y. Lu, J. Zhu, X. Zhang, Silica/polyacrylonitrile hybrid nanofiber membrane separators via sol-gel and electrospinning techniques for lithium-

ion batteries, J. Power Sources 313 (2016) 205–212, https://doi.org/10.1016/j.jpowsour.2016.02.089.
[22] F. Jiang, Y. Nie, L. Yin, Y. Feng, Q. Yu, C. Zhong, Core-shell-structured nanofibrous membrane as advanced separator for lithium-ion batteries, J. Membr. Sci. 510 (2016) 1–9, https://doi.org/10.1016/j.memsci.2016.02.067.
[23] J. Wang, J. Yang, L. Shen, Q. Guo, H. He, X. Yao, Synergistic effects of plasticizer and 3D framework toward high-performance solid polymer electrolyte for room-temperature solid-state lithium batteries, ACS Appl. Energy Mater. 4 (2021) 4129–4137, https://doi.org/10.1021/acsaem.1c00468.
[24] K.Z. Walle, L. Musuvadhi Babulal, S.H. Wu, W.C. Chien, R. Jose, S.J. Lue, J.K. Chang, C.C. Yang, Electrochemical characteristics of a polymer/garnet trilayer composite electrolyte for solid-state lithium-metal batteries, ACS Appl. Mater. Interfaces 13 (2021) 2507–2520, https://doi.org/10.1021/acsami.0c17422.